Numerical Predictions of Hydrodynamic Forces and Squat of Ships in Confined Waters

***Y. Liu[1], †L. Zou[1,2], Z. J. Zou[1,2], T.C. Lu[1] and J.X. Liu[3,4]**

[1]School of Naval Architecture, Ocean & Civil Engineering, Shanghai Jiao Tong University, Shanghai, China.
[2]Collaborative Innovation Center for Advanced Ship and Deep-Sea Exploration, Shanghai, China
[3]School of Navigation, Wuhan University of Technology, Hubei, China
[4]Hubei Key Laboratory of Inland Shipping Technology, Wuhan University of Technology, Wuhan, Hubei, China

*Presenting author: lucy261@sjtu.edu.cn
†Corresponding author: luzou@sjtu.edu.cn

Abstract

Due to the blockage effects in the flow, hydrodynamic performances of a ship in confined waterways are significantly different from those in deep waters. In particular, the hydrodynamic interactions between ship hull and sea bottom or bank wall in the vicinity tend to be more complicated. This gives rise to notable increases in hydrodynamic forces on the hull, along with more pronounced dynamic sinkage and trim where the ship squat phenomenon occurs. The predictions of hydrodynamic forces and ship squat are of great importance from the safe navigation point of view and are also challenging because of the remarkable viscous effects and flow separations in confined waters.

In this paper, an unsteady Reynolds-Averaged Navier Stokes (URANS) solver is applied to simulate the viscous flows around a tanker and a container ship in a confined tank, which is characterized by both shallow sea bottom and close side bank. In each case, the ship is moving along a straight course. The free surface elevation caused by the ship motion is captured by the Volume of Fluid method. In all simulations, the ship position during the motion is updated at each time step according to the computed hydrodynamic forces acting on the hull, from which the dynamic sinkage and trim of the ship is determined. A grid dependency study is performed so as to estimate the numerical error resulted from the grid discretization. The influences of water depth, ship-to-bank distance, ship speed and ship hull form on the hydrodynamic forces and squat of the ship are investigated through systematic computations. Numerical results are evaluated in combination with available experimental data. For the squat, additional data from a mathematical model are used for comparison. The hydrodynamic performances of the ships are generally in good agreement with the data. Furthermore, the mechanisms of the shallow water effects and bank effects involved in the confined waters are analyzed from the simulated flow field around the hulls.

Keywords: Hydrodynamic forces, squat, URANS simulation, shallow water, side bank

Introduction

A ship manoeuvring in confined waters usually experiences much larger hydrodynamic forces than in unrestricted waters due to the hydrodynamic interaction between the ship and the bottom/bank of the waterway. This hydrodynamic interaction has detrimental influence on ship manoeuvrability and may result in marine accidents such as collision or grounding. The ship undergoes dynamic sinkage and trim, notably at very small water depths, due to the hydrodynamic forces acting on the hull. This phenomenon is commonly termed as squat [1]. A decrease of the net Under Keel Clearance (UKC) resulted from squat may affect the ship's manoeuvrability dramatically, giving rise to the loss of ship control. In the latest report of International Towing Tank (ITTC) Manoeuvring Committee [2], it is pointed out that the knowledge of ship motions in confined waters remains a complex and challenging issue, which can be influenced by many different factors such as: free surface elevation, bank blockage, water depth, ship speed, etc. Therefore, to ensure a safe navigation, it is of great

importance to accurately predict the hydrodynamic forces acting on the ship manoeuvring in confined waters by taking the so-called shallow-water and bank effects into account.

Ship manoeuvring in confined waters has been studied in many ways for a long time. In general, most of the investigations rely on Experimental Fluid Dynamics (EFD) or model tests, theoretical and semi-theoretical methods [3, 4]. In Kazerooni [5], the squat of several ship models were measured and a regression formula was established from model tests results. The squat measurements in model tests of ships moving into and out of a lock chamber were conducted by Xu et al. [6]. Dand and Ferguson [7] established a semi-empirical method (D&F method) for the calculation of ship squat. Based on this theory, Latarie et al. [8] proposed a new mathematical model to predict the squat in rectangular cross sections. Gourlay et al. [9] calculated the dynamic sinkage and trim of modern container ships in confined waters by using slender-body method and Rankine-source method. Most recently, Mucha et al. [10] carried out model tests in confined waters, which was contributed as benchmark tests to the PreSquat-Workshop on Numerical Prediction of Ship Squat in Restricted Waters [11], aimed to benchmark the capabilities of available numerical methods for squat prediction and to increase the safety of manoeuvring ships.

Nowadays, with the rapid development of computer technique and Computational Fluid Dynamics (CFD) method, CFD-based numerical prediction of the hydrodynamic forces has become possible [12]. Especially, the viscous method, typically the Reynolds Averaged Navier-Stokes (RANS), is shown to be able to produce promising and comprehensive predictions of ship manoeuvrability. Many numerical investigations on the squat of ships advancing in confined waterways have been conducted, such as Toxopeus et al. [13], Kaidi et al. [14], Tezdogan et al. [15] and Linde et al. [16]. Moreover, Zou and Larsson [17] utilized a RANS solver to investigate the bank effects on a tanker hull in two canals. A similar simulation for a bulk carrier passing a lock was conducted by Wang and Zou [18]. Liu et al. [19] assessed the ship manoeuvring stability in Planar Motion Mechanism (PMM) tests taking the ship-bank distance into account. Wang et al. [20] numerically simulated the berthing manoeuvre of a ship in the prescribed translational motion.

In this paper, a numerical investigation is performed aiming to find an efficient numerical method for the ship squat and hydrodynamic forces predictions in confined waters combing the comparisons with available experimental data.

Ship geometry and computational cases

Two benchmark ship models are considered in the present study, namely, KVLCC2 tanker and KCS container ship. Fig. 1 presents their line plans without the scale drawn. Geometries are available at the website of SIMMAN2014 [21]. Main particulars of the two ships are given in Table 1.

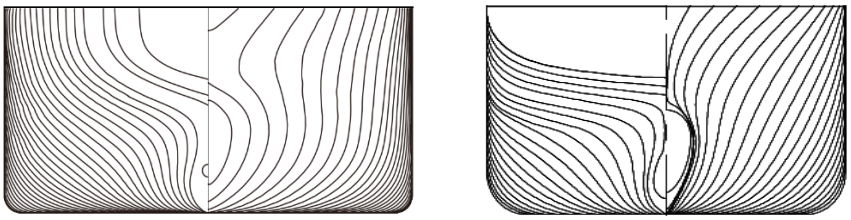

a) KVLCC2 b) KCS

Figure 1. Line plans of ships

Table 1. Main particulars of the three ships

Particulars	KVLCC2	KCS
Length between perpendiculars L_{pp} (m)	320.0	230.0
Breadth B (m)	58.0	32.2
Design Draft T (m)	20.8	10.8
Block coefficient C_B (-)	0.8098	0.651
Displacement ∇ (m^3)	312,622	52,022
Moment of Inertia K_{xx}/B	0.4	0.4
Moment of Inertia K_{yy}/L_{pp}, K_{zz}/L_{pp}	0.25	0.25
Wet surface area S (m^2)	27194	9424
Vertical Center of Gravity (from keel) KG(m)	18.6	7.28
LCB (%L_{pp}), fwd+	3.48	-1.48

In the numerical computations, the same test conditions are used as in the experiments to ensure direct comparisons. Benchmark tests of KVLCC2 hull in shallow water in model scale (scale factor λ=75) are obtained from Flanders Hydraulics Research (FHR) [22]. The ship model was towed at a constant forward speed U along different lateral positions y_{wall} in a rectangular tank (See Fig. 2). The width W of the tank section is varied from 2.5B up to the entire width of the towing tank (9.05B, 7m). Also, a range of water depths varied from 1.1T to 3T was tested. The blockage factor m_b=(B×T)/(h×W) is defined as the ratio of the ship's underwater cross-sectional area at mid-ship to the cross-sectional area of the waterway. The water depth h, tank width W and the forward speed U are summarized in Table 2.

The computations of KCS model (λ=40) are conducted for h=1.3T, 1.6T at 0.73m/s forward speed and for 1.2T water depth at 0.82m/s respectively. These conditions are identical to the experiments carried out at the Development Center for Ship Technology and Transport Systems (DST) in Duisburg, Germany [23, 24]. The bank effect is neglected for this ship model. It will be mainly used for comparing the ship resistance and squat predictions with KVLCC2 model at the same Froude depth number Fr_h (=$U/\sqrt{gh}$).

Table 2. Overview of the test conditions for KVLCC2 model

U (full scale)	U	W	h	m_b	Fr_h	y	y_{wall}
Knot	m/s	-	-	-	-	m	m
7	0.416	*9.05B*	*1.2T*	0.092	0.230	0	0
			1.5T	0.074	0.203		
			3T	0.037	0.146		
15.5	0.921	*9.05B*	*1.2T*	0.092	0.510	0	0
			1.5T	0.074	0.456		
			3T	0.037	0.323		
8	0.475	5B	1.1T	0.182	0.275	0	0
			1.35T	0.148	0.248		
			1.5T	0.133	0.235		
8	0.475	5B	1.5T	0.133	0.235	1.526	0.02
						1.352	B/4
						0.773	B

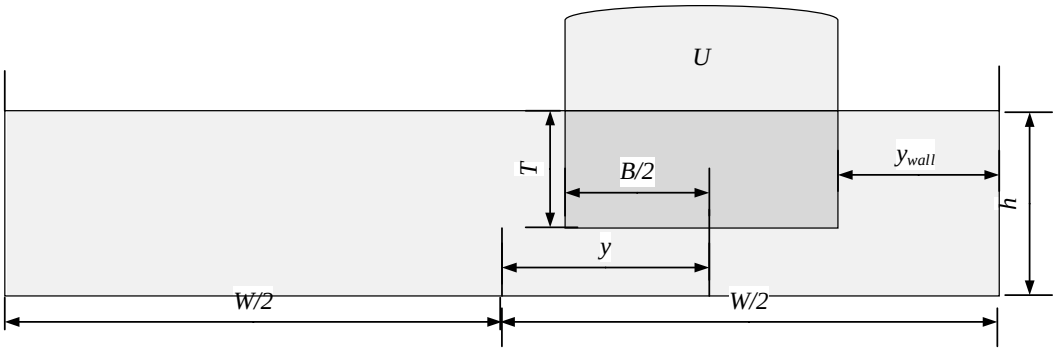

Figure 2. The variables in a cross section of the tank

Numerical Models

Governing equations

The viscous flow involved in the manoeuvring tests can be treated as incompressible, and is governed by the Navier-Stokes (N-S) equations. After averaging the N-S equations over time, the unsteady Reynolds Averaged Navier-Stokes (RANS) equations can be written as follows:

$$\begin{cases} \dfrac{\partial u_i}{\partial x_i} = 0 \\ \rho \dfrac{\partial u_i}{\partial t} + \rho u_j \dfrac{\partial u_i}{\partial x_j} = -\dfrac{\partial p}{\partial x_i} + \dfrac{\partial}{\partial x_j}\left(\mu \dfrac{\partial u_i}{\partial x_j} - \rho \overline{u_i' u_j'} \right) \end{cases} \quad (i, j = 1, 2, 3) \tag{1}$$

where $x_{i,j}$ (i, j=1, 2, 3, $i \neq j$) is the ith or jth component of the fixed coordinate system, ρ is the density of fluid, $u_{i,j}$ (i, j=1, 2, 3, $i \neq j$) is ith or jth mean velocity component, p is the mean pressure, μ is the viscosity and $-\rho \overline{u_i' u_j'}$ is the Reynolds stress which needs to be solved through turbulence modelling.

Numerical Methods

To simulate the viscous flow, the CFD software STAR-CCM+ [25] is applied in the present study to solve the RANS equations. A Finite Volume Method (FVM) is used to discretize the flow domain into a finite number of control volumes (CVs). The temporal discretization is based on a first-order Euler difference, and the spatial discretization is performed with second-order upwind scheme for the convection term and secondary gradient contribution for the diffusion term.

The air-water interface is captured using the Volume of Fluid (VOF) method [26]. VOF assumes a common velocity and pressure field for both phases within a single CV, and monitors the phase fraction. The governing equations for mass and momentum continuity in a single-phase flow are thus solved for an equivalent fluid, whose physical properties (density and laminar viscosity) are functions of the constituent phase's properties and volume fractions. The transport of volume fraction is described by an additional conservation equation:

$$\frac{\partial \alpha}{\partial t} + \frac{\partial (u_i \alpha)}{\partial x_i} = 0 \tag{2}$$

where α represents the volume fraction, indicating the relative proportion of fluid in each cell; its value is always between 0 and 1. The High Resolution Interface Capturing (HRIC) convection discretization scheme [27] is used to improve the VOF interface tracking capabilities.

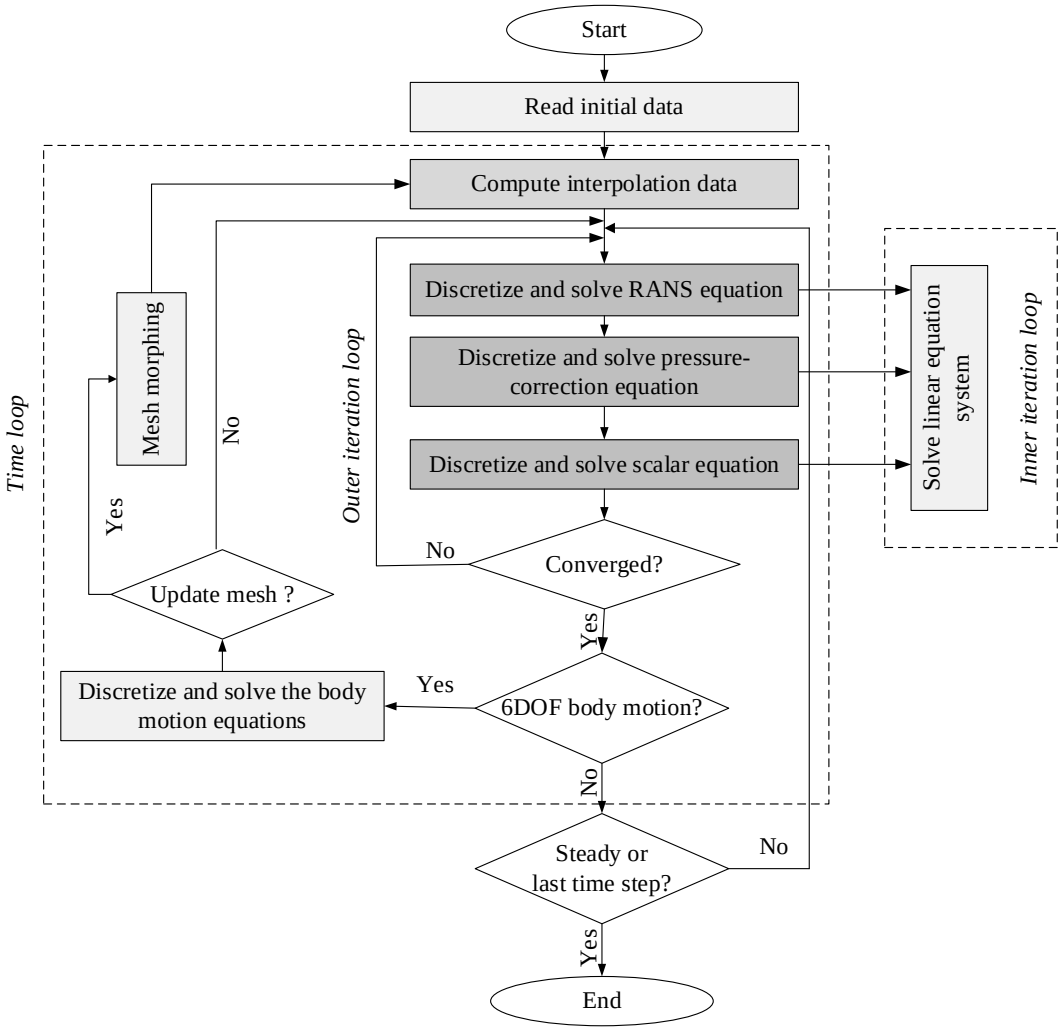

Figure 3. Main flow chart in the STAR-CCM+ solver

Mean flow quantities near the solid wall are simulated according to an all y^+ wall treatment where blended wall function is adopted. This approach is flexible as it's capable of handling a range of local grid refinement levels near the wall. If the grid is fine enough ($y^+<1$), the viscous sublayer is resolved and and thus the wall shear stress is computed as it would be in a laminar flow. If the grid is coarse ($y^+> 30$), the wall law is equivalent to a logarithmic profile. The SIMPLE algorithm [28] is employed for pressure-velocity coupling. Moreover, the RANS equations are closed with *k*-ε turbulence model [29]. Particularly, the sinkage and trim motion are specified with the "Dynamic Fluid body Interaction (DFBI) morphing" module. It involves actual displacement of the grid vertices, and can use control points and their associated displacements to generate an interpolation field throughout the region, which can model the 6-DOF motion of a rigid body within the fluid system. Then the resultant force and

moment acting on the body due to all influences are calculated, and the flow field is updated to find the new position and orientation of the ship. More details about the DFBI formulation can be found in Ohmori [30]. For resistance computations in calm water, the time step is determined by 0.05-0.01L_{pp}/U in accordance with the related guidelines of ITTC[31]. A much smaller time step (<0.002L_{pp}/U) is used in the present work since the flow in the confined water condition is more unstable. A general flow chart of this solver is indicated in Fig. 3.

Computational setup and grid generation

The computational domain and general grid distributions for the case of KVLCC2 model at h/T=1.5 and W=5B are given in Fig. 4. The bottom position of the domain is determined according to the corresponding water depth, and the tank width is related to the test conditions in Table 2. The computational domain in the numerical tests is made by eight boundaries: inlet plane, outlet plane, hull surface, top plane, tank bottom, as well as two side walls representing the bank of the tank. It should be noted that in the W=9.05B case, only a half of the domain is modeled since this case represents the hull located in the center of the tank, indicating a symmetry flow configuration. The fluid domain extends 1.5L_{pp} from the bow to the inlet plane, 3.5L_{pp} from the aft-perpendicular to the outlet plane and 0.33 L_{pp} from the free surface to the top plane. The water depth and tank width in the domain vary in the following systematic computations.

As to the adopted boundary conditions in the computations, the velocity inlet condition is set on the inlet and top plane where the boundary pressure is extrapolated by using reconstruction gradients. The pressure outlet condition is used on outlet plane where the boundary pressure is governed by a field function which monitors the instantaneous pressure on, above and below the free surface at the boundary. The symmetry condition is set on the symmetry plane in the half domain case where the shear stress is zero. A no slip condition is satisfied on the hull and slip wall condition on the side walls. It should be noted that in shallow water cases, the effect of the boundary layer on the tank bottom greatly influences the flow in the gap between the ship and bottom, so a moving no-slip condition is used on the bottom. The two side bank walls are also set as moving no-slip wall in the narrow bank case (W<9.05B). The pressure resistance fluctuation is usually found to be caused by the wave reflection at the non-physical side boundaries. Therefore, a numerical damping method with a damping length of 10m is applied on the inlet and outlet boundaries to remove the fluctuation. Furthermore, the release and ramp time are up to 20s to allow enough time for the fluid flow to be stable.

Fig. 5 provides a closer look at the grid cells around the ship hull. As shown in Fig. 5, the grid is refined near the free surface, tank bottom, hull surface, bank sides and in the wake region to ensure that the complex flow features are appropriately captured. The grid refinements in these zones are achieved using volumetric controls. Orthogonal prismatic cells are generated next to the hull, tank bottom surfaces and side walls to improve the accuracy of the flow resolution. The prism layer is not used on the two side surfaces in the wide tank condition (W=9.05B), where the blockage effect is minor. To avoid numerical difficulty related to the DFBI morphing approach as much as possible for shallow water cases, y^+ is larger than 30 so as to use wall function on the tank bottom and the close side tank wall, while y^+ is smaller than 1 at the hull surface to get a more precise flow field simulation near the ship.

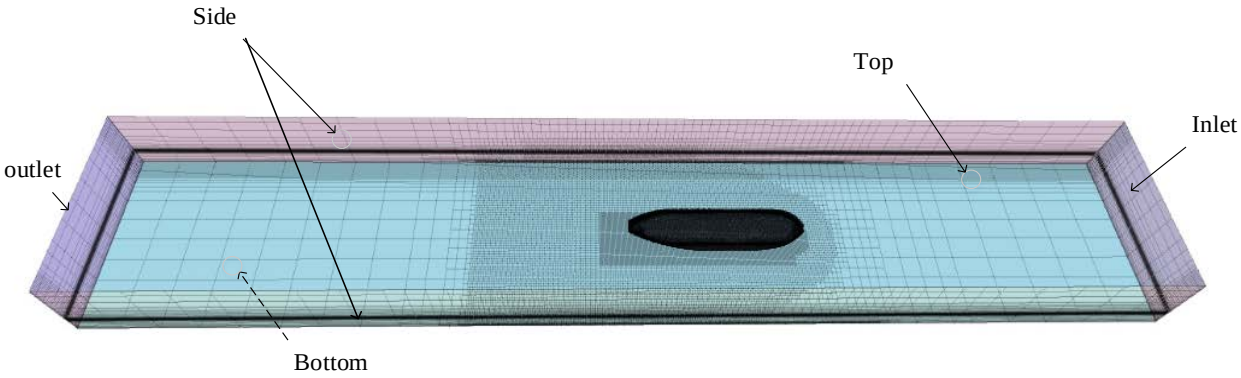

Figure 4. Overview of computational domain

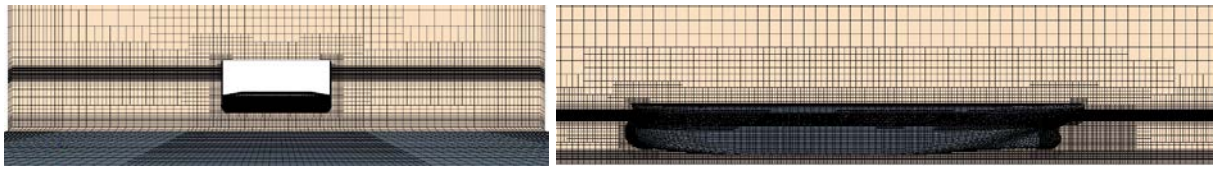

(a) (b)

Figure 5. Grid structure around ship and bottom in shallow water
(a) cross section at mid-ship (b) longitudinal section at *y*=0

Results and Discussion

Grid dependency study for KVLCC2

The purpose of grid dependency study is to estimate the numerical error and uncertainty resulted from the grid discretization. In this paper, this study is conducted following the Grid Convergence Index(GCI) method [32]. It is applicable for unstructured grid and only requires the grid refinement to be done systematically. Therefore, all grid quantities are given as percentages in terms of a base size, in order to refine the grid in a more systematic way. The case of KVLCC2 at h=1.2T, 9.05B bank width and the 0.921m/s forward speedis chosen for the study. Only half of the computational domain is used to reduce the calculation cost. Three grid sets (coarse, medium and fine) are adopted in the study and the grid refinement is achieved by applying a refinement factor $r_G=\sqrt{2}$ to the base size. The fine grid (No.1) consists of approximately 2.9M cells; the medium grid (No.2) contains about 1.3M; and about 0.69M in the coarse grid (No.3). The changes in solutions between two successive grids are defined as: $\varepsilon_{32} = \phi_3 - \phi_2$, $\varepsilon_{21} = \phi_2 - \phi_1$. The apparent order p of the method is expressed by:

$$p = \frac{1}{\ln(r_G)} \left| \ln \left| \varepsilon_{32} / \varepsilon_{21} \right| \right| \tag{3}$$

The extrapolated values ϕ_{ext}^{21} can be calculated by:

$$\phi_{ext}^{21} = (r_G \phi_1 - \phi_2)/(r_G^P - 1) \tag{4}$$

The approximate relative error between medium-fine solutions e_a^{21} and extrapolated relative error e_{ext}^{21} can be computed as follows:

$$e_a^{21} = \left| \frac{\phi_1 - \phi_2}{\phi_1} \right| \tag{5}$$

$$e_{ext}^{21} = \left| \frac{\phi_{ext}^{21} - \phi_1}{\phi_{ext}^{21}} \right| \tag{6}$$

The fine-grid convergence index GCI_{fine}^{21} is calculated by:

$$GCI_{fine}^{21} = \frac{1.25 e_a^{21}}{r_G^P - 1} \tag{8}$$

The total resistance (R_t) of a ship is mainly composite of two components: the pressure resistance (R_p) and the frictional resistance (R_f). The computed values of R_p, R_f, R_t and the ship sinkage σ of the coarse, medium and fine grids are given in Table 3. The e_a^{21} results show that all the resistances have small approximate relative errors. Moreover, the values of GCI in all coefficients are no more than 5%. From the grid dependency study, the observed errors in all grid sets are not large, thus a medium grid density is chosen to maintain an affordable computation cost.

Table 3. Grid convergence parameters

	Pressure resistance R_p (N)	Frictional resistance R_f (N)	Total Resistance R_t(N)	Sinkage σ (mm)
ϕ_3	14.23	7.76	21.99	24.59
ϕ_2	14.44	8.18	22.62	24.11
ϕ_1	14.81	8.20	23.02	23.76
p	1.72	9.05	1.37	1.00
ϕ_{ext}^{21}	15.27	8.20	23.66	22.94
e_a^{21} %	2.53	0.23	1.71	1.43
e_{ext}^{21} %	3.01	0.01	2.73	3.58
GCI_{fine}^{21} %	3.89	0.01	3.51	4.32

For more clear comparison, the resistance R_p, R_f and R_t and sinkage σ are expressed in non-dimensional form in the next section. The resistance coefficients C_p, C_f and C_t are achieved by dividing each term by $0.5\rho U^2 S$ and the sinkage σ' by L_{pp}, respectively.

KVLCC2

1. W=9.05B-centred ship

Firstly, the predicted total resistance and sinkage of KVLCC2 model in a wide tank (W=9.05B) at three different water depths: 1.1T, 1.35T and 1.5T are compared to the experimental data [22] and the results computed from D&F mathematical formula, which is a semi-empirical method based on the Bernoulli Equation[7]. As shown in Fig. 6, the overall computed resistances at different water depths agree well with the measurements and the sinkage also indicates satisfactory agreement.

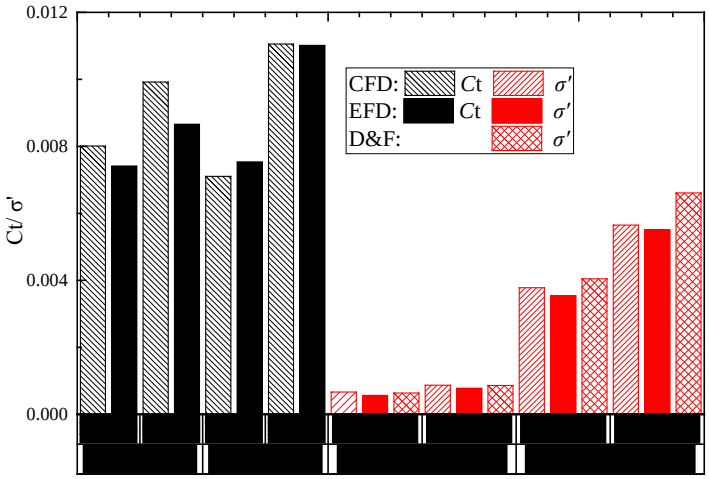

Figure 6. Comparison with experimental data [22] and D&F mathematical model

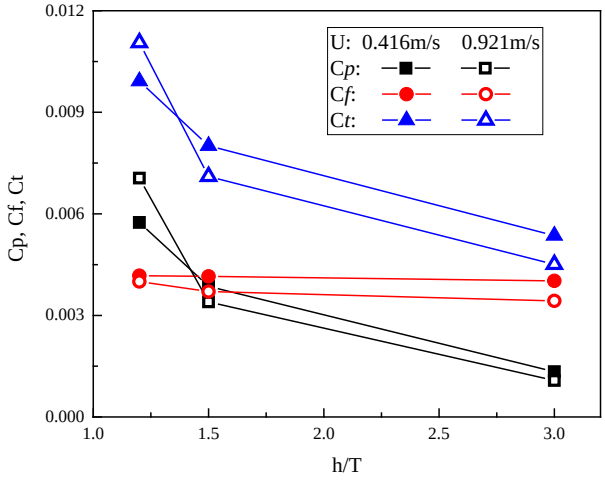

Figure 7. Resistance coefficients at different water depths and forward speeds

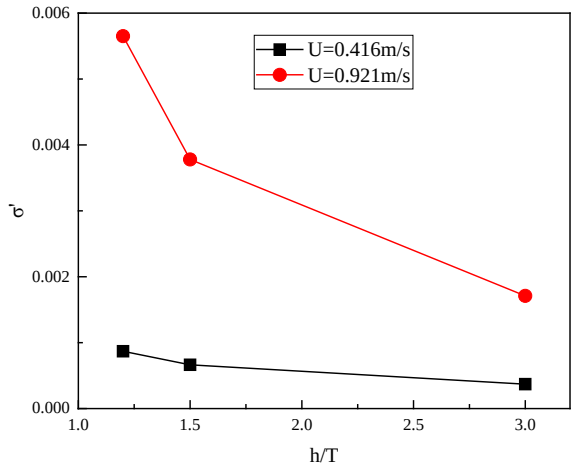

Figure 8. Sinkage coefficients at different water depths and forward speeds

The numerical results of resistance and sinkage with the same tank width but different Fr_h are shown in Fig. 7-8. It can be seen that all the resistance coefficients-C_p, C_f and C_t increase as the water depth decreases at the same forward speed, among which the increase in C_f is less. The sinkage coefficient increases rapidly as Fr_h becomes larger.

2. *W*=5*B*-centred ship

The results of resistance and sinkage coefficients of KVLCC2 with a narrow tank width (*W*=5*B*) are given in Fig. 9 and Fig. 10, respectively. The results of sinkage are also compared with the experimental data from Lataire et al. [8] and the computed results from D&F mathematical formula [7]. The computed sinkage coefficients qualitatively follow the same trend as the measurements with slight under-predictions. Results from the D&F method also indicate a similar trend, but there are large deviations from either computation or experiment. The difference between computed and measured sinkage is due to the fact that the sinkage values are small, which are difficult to capture precisely. It might be also caused by the propulsion effects. In the experiments, the ship model is tested with a rotating propeller, while in the numerical simulations no appendage is equipped.

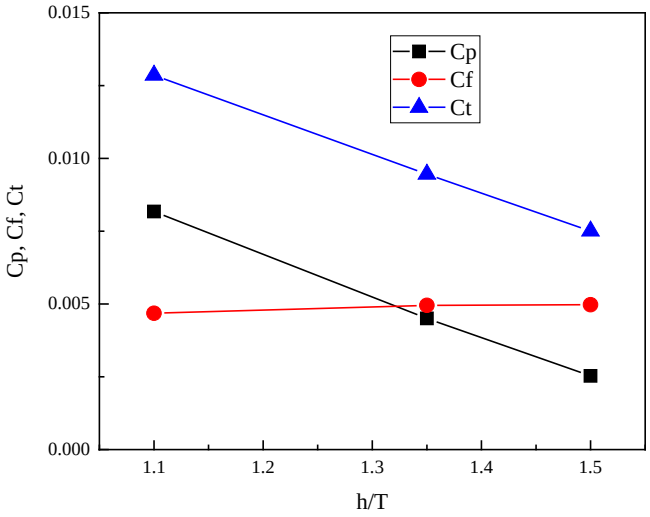

Figure 9. Resistance coefficients in the 5*B* tank width case

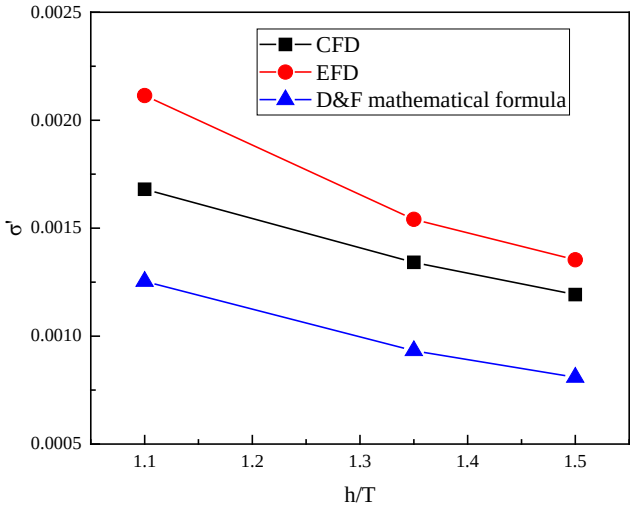

Figure 10. Sinkage coefficient in the 5*B* tank width case

3. *W*=5*B*-Offset ship longitudinal central position

To investigate the bank effects, three configurations with different ship-bank distances are simulated. The distance y_{wall} (see Fig. 3 and Table 2) is defined as:

$$y_{wall} = \frac{W}{2} - \frac{B}{2} - y \tag{9}$$

The lateral position y specifies the distance between the centerlines of the ship and the tank.

The resistance coefficients are given in Fig. 11. In this investigation, two more influential quantities are examined, namely, sway force Y and yaw moment N (see Fig. 11). The two hydrodynamic forces are nondimensionlized by $0.5\rho U^2 L_{pp} T$ and $0.5\rho U^2 L_{pp}^2 T$, respectively. The results show that hydrodynamic forces are affected by the y_{wall}. These forces are larger when the ship is getting closer to the bank. The sinkage coefficients are shown in Fig. 12 and compared with the mathematical model from Lataire et al. [8]. The sinkage predicted by CFD method is lower than that the experimental data in [8], since the mathematical model considers the propeller effects.

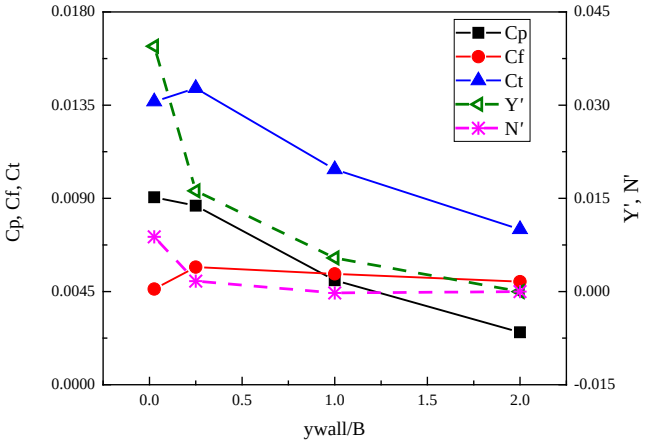

Figure 11. Resistance, sway force, yaw moment coefficients vs. y_{wall}/B

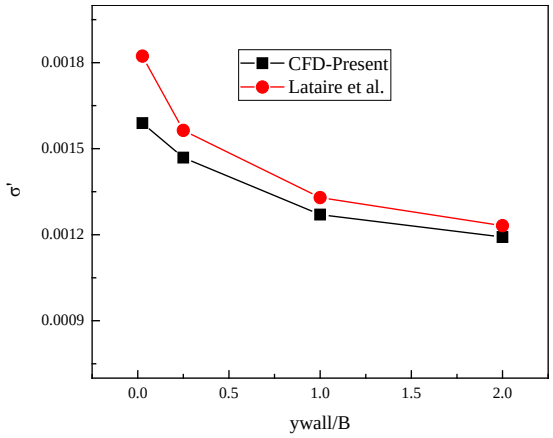

Figure 12. Sinkage coefficients vs. y_{wall}/B

To gain a deeper insight into the physical mechanism in the hydrodynamic forces on the ship, pressure distributions on the hull and the tank bottom surface, along with the free surface elevation are discussed in Figs. 13-14. As shown in Fig. 13, there are significant differences between the pressure distributions at different water depths. For the shallowest case, a distribution of significant suction pressures can be observed on the aft and fore part of the hull. The Kelvin wave pattern can be seen for the three cases.

The bank effects are clearly indicated in Fig. 14. The hull surface facing the near bank side has a larger suction pressure and it is clearly noticed for the case with y_{wall}=0.02. The pressure increases as positive at the bow which pushes the ship to the tank centre.

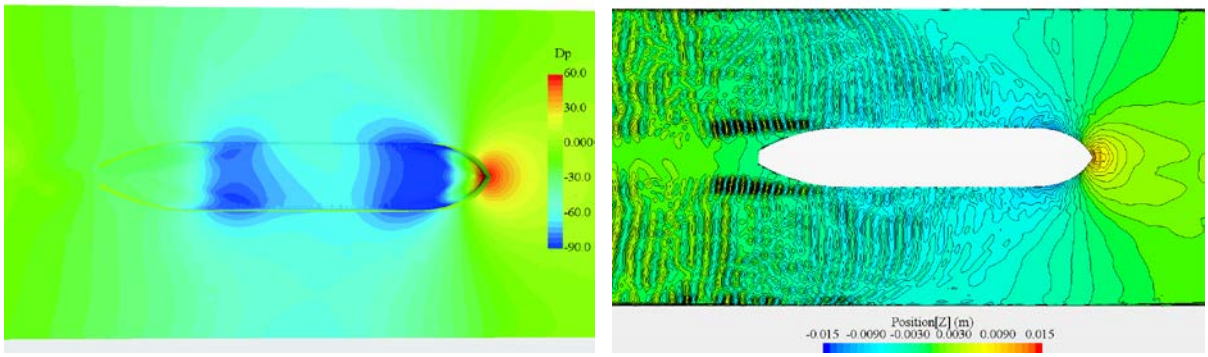

a) h/T=1.1

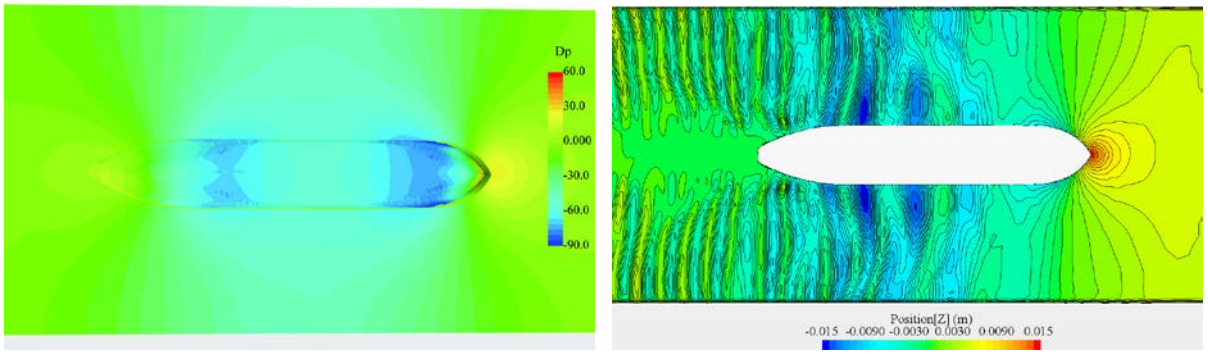

b) h/T=1.35

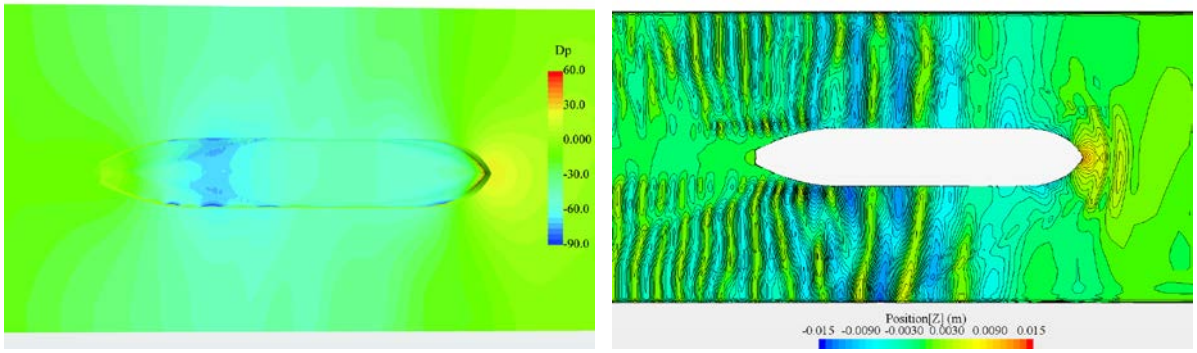

c) h/T=1.5

Figure 13. Dynamic pressures and wave elevation at different water depths (Left: dynamic pressure; right: wave elevation)

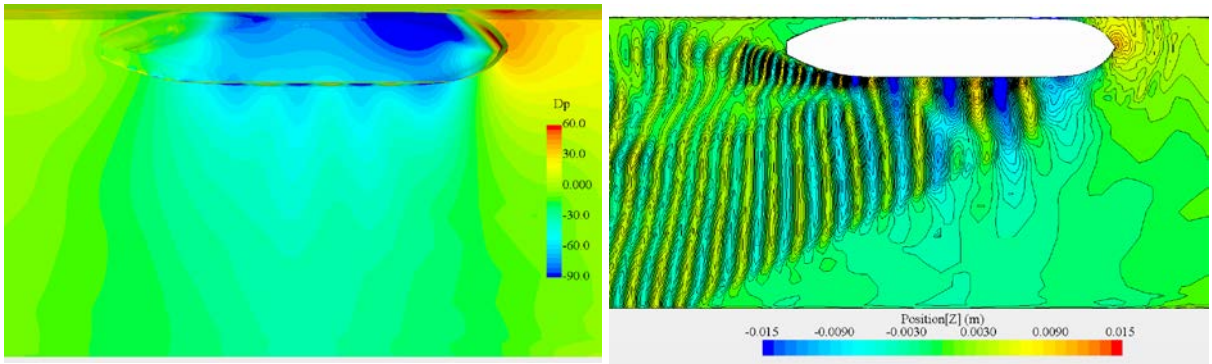

a) y_{wall}=0.02B

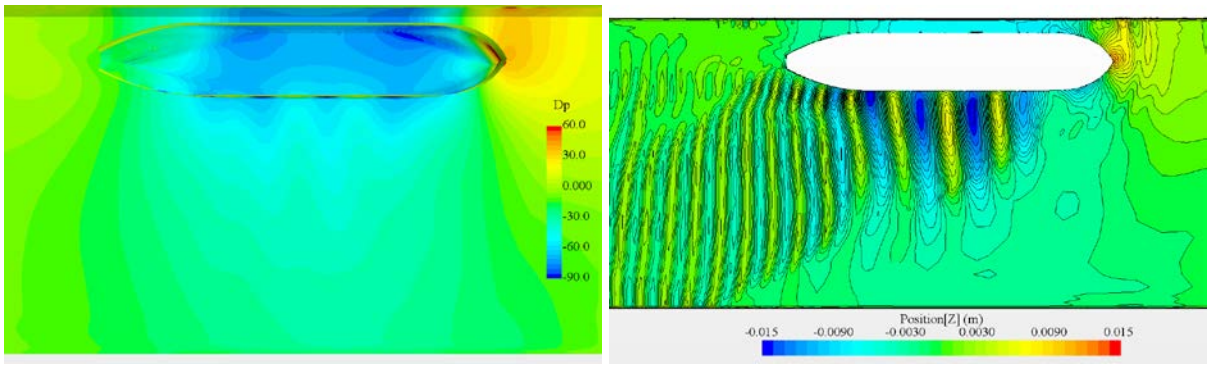

b) y_{wall}=0.25B

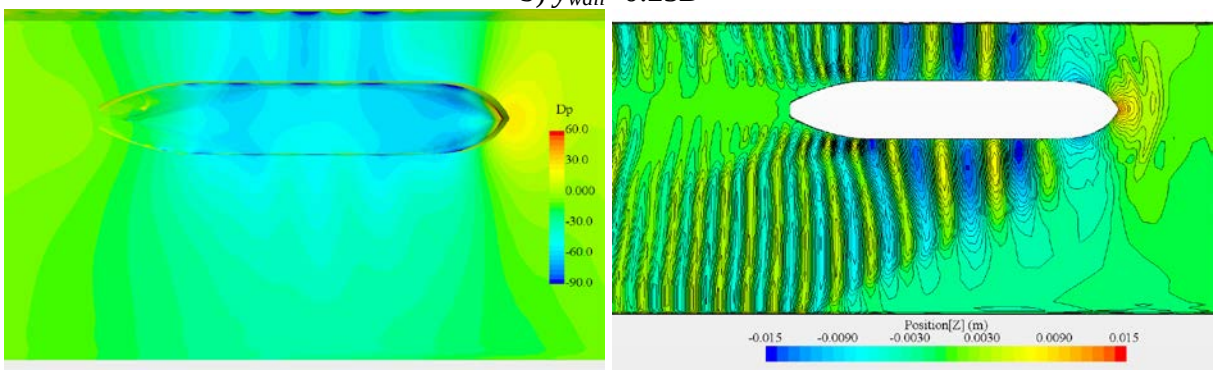

c) y_{wall}=B

Figure 14. Dynamic pressure and wave elevation under different y_{wall} (Left: dynamic pressure; right: wave elevation)

KCS

Similarly, the predicted total resistance and sinkage coefficients of KCS model using the RANS method are compared to the experimental data [24]. As shown in Fig. 15, the overall agreement between EFD and CFD is good, except for the C_t at h/T=1.2.

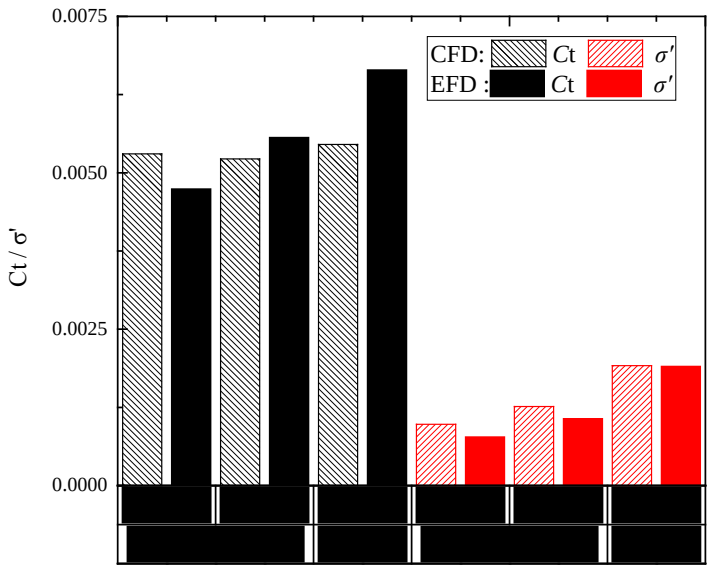

Figure 15. Comparison with experimental data [24]

Then the frictional, pressure, total resistance coefficients and the sinkage of the KCS model are compared with those of KVLCC2 model at the same Fr_h. That is to say, the motion and

the resistance of KCS model at three different water depth ratio h/T: 1.2, 1.5 and 3.0 at the forward speed 0.874m/s in the range of Froude depth numbers Fr_h=0.51, 0.456, 0.323 are simulated corresponding to the KVLCC2 model at the 0.921m/s forward speed at the same three water depth ratios. The comparisons are shown in Fig. 16-17. It can be seen that all the resistance coefficients and the sinkage coefficients of KVLCC2 are larger than those of KCS at the same Fr_h. Given that in model tests the KVLCC2 is shorter but has larger C_B than KCS, it seems that the blunt hulls will be more affected by the shallow water effects.

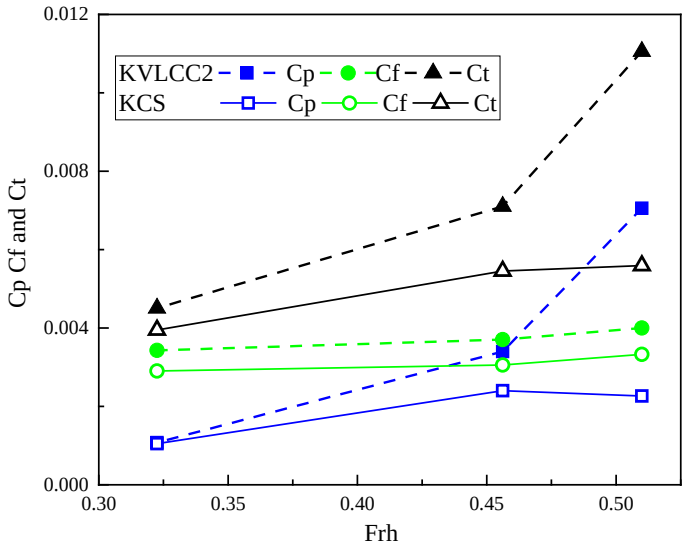

Figure 16. Resistance coefficients comparison between KCS and KVLCC2

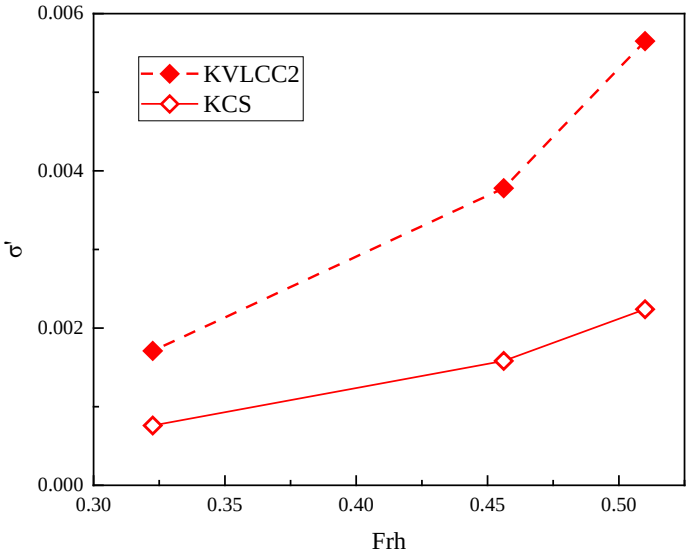

Figure 17. Sinkage coefficients comparison between KCS and KVLCC2

Conclusions

In this paper, a numerical method based on RANS equation is proposed to study the influence of tank width and water depth in terms of the shallow-water and bank effects. The sinkage and resistance results of the three benchmark ships obtained from the CFD simulations are presented in a range of ship speeds at different water depths. The numerical results of squat were also compared to those from available experiments. The general agreement between the resistance predictions by experimental measurements and numerical simulations is satisfactory. For KVLCC2, the pressure resistance is dominant in the wide tank width case.

However, the resistance coefficients of KCS are all smaller than those of KVLCC2 at the same Fr_h. The agreement in the squat predictions for both hulls is also promising. The mid-ship sinkage is dominated by the local pressure along the parallel middle body which can be captured well by the present CFD method. Therefore, a better understanding of the hydrodynamic performances for ships travelling in confined waters is obtained.

Acknowledgments

The work described in this paper was supported by grants from the National Natural Science Foundation of China (NSFC) (No.: 51479156 and 51309152). And the authors would like to thank the reviewers for their constructive and valuable comments which lead to the better presentation of this paper.

References

[1] Briggs, M. J., Vantorre, M., Uliczka, K. and Debaillon, P. (2010) Prediction of squat for underkeel clearance, *Handbook of Coastal and Ocean Engineering World Scientific Publishing Company*, 723-774.

[2] International Towing Tank Conference Maneuvering Committee.(2014) *Final report and recommendations to the 27th ITTC, 27th International Towing Tank Conference(ITTC)*, Copenhagen, Denmark.

[3] Ankudinov, V., Daggett, L., Huval, C. and Hewlett, C.(1996) *Squat predictions for manoeuvring applications, the 7th International Conference on Marine Simulation and Manoeuvrability (MARSIM)*, Copenhagen, Denmark.

[4] Briggs, M. J. (2006). Ship squat predictions for ship/tow simulator.

[5] Kazerooni, M. F. and Seif, M. S. (2014) Experimental evaluation of ship squat in shallow waters, *Journal of the Brazilian Society of Mechanical Sciences and Engineering* **36**, 559-569.

[6] Xu, J. C., Xuan, G. X., Li, Y., Li, Z. H., Hu, Y., Jin, Y. and Huang, Y. (2016) Study on the squat of extra-large scale ship in the Three Gorges ship lock, *Ocean Engineering* **123**, 65-74.

[7] Dand, I. and Ferguson, A. (1973) Estimatinq the bow and stern sinkage of a ship underway in shallow water, *The Naval Architect*.238.

[8] Lataire, E., Vantorre, M. and Delefortrie, G. (2012) A prediction method for squat in restricted and unrestricted rectangular fairways, *Ocean Engineering* **55**, 71-80.

[9] Gourlay, T. P., Ha, J. H., Mucha, P. and Uliczka, K.(2015) *Sinkage and trim of modern container ships in shallow water, the 22nd Australasian Coastal and Ocean Engineering Conference*, Auckland, New Zealand.

[10] Mucha, P., Moctar, O. E. and Böttner, C. U. (2014) Technical note: PreSquat–Workshop on numerical prediction of ship squat in restricted waters, *Ship Technology Research* **61**, 162-165.

[11] https://www.uni-due.de/IST/ismt_presquat_test.shtml. (2014) *Introduction-Dynamic Squat Test Parameter, Presquat.*

[12] Stern, F., Yang, J. M., Wang, Z. Y., Sadat-Hosseini, H., Mousaviraad, M., Bhushan, S. and Xing, T. (2013) Computational ship hydrodynamics: Nowadays and way forward, *International Shipbuilding Progress* **60**, 3-105.

[13] Toxopeus, S. L., Simonsen, C. D., Guilmineau, E., Visonneau, M., Xing, T. and Stern, F. (2013) Investigation of water depth and basin wall effects on KVLCC2 in manoeuvring motion using viscous-flow calculations, *Journal of Marine Science and Technology* **18**, 471-496.

[14] Kaidi, S., Smaoui, H. and Sergent, P. (2017) Numerical estimation of bank-propeller-hull interaction effect on ship manoeuvring using CFD method, *Journal of Hydrodynamics, Ser B* **29**, 154-167.

[15] Tezdogan, T., Incecik, A. and Turan, O. (2016) A numerical investigation of the squat and resistance of ships advancing through a canal using CFD, *Journal of Marine Science and Technology* **21**, 86-101.

[16] Linde, F., Ouahsine, A., Huybrechts, N. and Sergent, P. (2016) Three-Dimensional Numerical Simulation of Ship Resistance in Restricted Waterways: Effect of Ship Sinkage and Channel Restriction, *Journal of Waterway, Port, Coastal, and Ocean Engineering* **143**.

[17] Zou, L. and Larsson, L. (2013) Computational fluid dynamics (CFD) prediction of bank effects including verification and validation, *Journal of Marine Science and Technology* **18**, 310-323.

[18] Wang, H. Z. and Zou, Z. J. (2014) Numerical prediction of hydrodynamic forces on a ship passing through a lock, *China Ocean Engineering* **28**, 421-432.

[19] Liu, H., Ma, N. and Gu, X. C. (2016) Numerical simulation of PMM tests for a ship in close proximity to sidewall and maneuvering stability analysis, *China Ocean Engineering* **30**, 884-897.

[20] Wang, H. M., Li, X. H., Chen, L. and Sun, X. J. (2016) Numerical study on the hydrodynamic forces on a ship berthing to quay by taking free-surface effect into account, *Journal of Marine Science and Technology* **21**, 601-610.
[21] http://www.simman2014.dk/.(2014) *Workshop on Verification and Validation of Ship Manoeuvring Simulation Methods (SIMMAN), Copenhagen, Denmark.*
[22] Delefortrie, G., Eloot, K. and Mostaert, F. (2012) *SIMMAN 2013: Execution of model tests with KCS and KVLCC2*. Antwerp, Belgium.
[23] Mucha, P., Deng, G., Gourlay, T. and Moctar, O. E.(2016) *Validation Studies On Numerical Prediction Of Ship Squat And Resistance In Shallow Water*, the *4th International Conference on Ship Manoeuvring in Shallow and Confined Water (MASHCON): Ship - Bottom Interaction*, Hamburg, Germany.
[24] Mucha, P. and Moctar, O. E. (2014) *Numerical Prediction of Resistance and Squat for a Containership in Shallow Water, the 17th Numerical Towing Tank Symposium*, Marstrand, Sweden.
[25] STAR-CCM+ User Guide. (2014) CD-Adapco.
[26] Hirt, C. W. and Nichols, B. D. (1981) Volume of fluid (VOF) method for the dynamics of free boundaries, *Journal of Computational Physics* **39**, 201-225.
[27] Muzaferija, S., Peric, M., Sames, P. and Schellin, T.(1998) *A two-fluid Navier-Stokes solver to simulate water entry, the 22nd symposium on naval hydrodynamics(ONR),* Washington, DC., USA.
[28] Patankar, S. V. and Spalding, D. B. (1972) A calculation procedure for heat, mass and momentum transfer in three-dimensional parabolic flows, *International Journal of Heat and Mass Transfer* **15**, 1787-1806.
[29] Launder, B. E. and Spalding, D. B. (1974) The numerical computation of turbulent flows, *Computer Methods in Applied Mechanics and Engineering* **3**, 269-289.
[30] Ohmori, T. (1998) Finite-volume simulation of flows about a ship in maneuvering motion, *Journal of Marine Science and Technology* **3**, 82-93.
[31] ITTC-Recommended Procedures and Guidelines. (2011) Practical Guidelines for Ship CFD Applications.
[32] Celik, I. B., Ghia, U., Roache, P. J. and Freitas, C. J. (2008) Procedure for estimation and reporting of uncertainty due to discretization in CFD applications, *Journal of Fluids Engineering-Transactions of the ASME* **130**.